A multi-scale porous scaffold fabricated by a combined additive manufacturing and chemical etching process for bone tissue engineering

Cijun Shuai[1,2], Youwen Yang[1,2], Pei Feng[1], Shuping Peng[3], Wang Guo[1], Anjie Min[4], Chengde Gao[1*]

[1] State Key Laboratory of High Performance Complex Manufacturing, College of Mechanical and Electrical Engineering, Central South University, Changsha 410083, China

[2] Jiangxi University of Science and Technology, Ganzhou 341000, China

[3] The Key Laboratory of Carcinogenesis and Cancer Invasion of the Chinese Ministry of Education, the Key Laboratory of Carcinogenesis of the Chinese Ministry of Health and Cancer Research Institute, Xiangya Hospital, Central South University, Changsha 410078, China

[4] Department of Oral and Maxillofacial Surgery, Xiangya Hospital, Central South University, Changsha 410008, China

Abstract: It is critical to develop a fabrication technology for precisely controlling an interconnected porous structure of scaffolds to mimic the native bone microenvironment. In this work, a novel combined process of additive manufacturing (AM) and chemical etching was developed to fabricate graphene oxide/poly(L-lactic acid) (GO/PLLA) scaffolds with multi-scale porous structure. Specially, AM was used to fabricate an interconnected porous network with pore sizes of hundreds of microns. And the chemical etching in sodium hydroxide solution constructed pores with several microns or even smaller on scaffolds surface. The degradation period of the scaffolds was adjustable via controlling the size and quantity of pores. Moreover, the scaffolds exhibited surprising bioactivity after chemical etching, which was ascribed to the formed polar groups on scaffolds surfaces. Furthermore, GO improved the mechanical strength of the scaffolds.

Keywords: multi-scale pores; scaffolds; additive manufacturing; chemical etching; PLLA

1. Introduction

To fabricate a multi-scale and interconnected porous structure for scaffolds is a key challenge in bone tissue engineering[1–3]. In general, pores with hundreds of microns (macro pores) are necessary for vascularization and tissue ingrowth[4–6]. On the other hand, pores with several microns or even smaller (micro pores) on the scaffolds surface allow facile communication between the cells and scaffolds, thereby promoting extracellular matrix formation[7]. Moreover, the micro pores on surface provide more sites for apatite formation and cell adhesion. In addition, the degradation rate of scaffolds should be adjustable to enable synchronous replacement of the scaffold with the cells and extracellular matrix[8]. And an adequate mechanical strength is also required to provide structural support for the new tissue[9,10]. Therefore, it is of great importance to develop scaffolds with suitable porous structure, degradation rate and mechanical strength to meet the multiple requirements.

To obtain the porous structure of scaffolds, substantial efforts have been devoted to exploring scaffolds fabrication methods, including freeze-drying[11,12], gas forming[13] and polymeric sponge[14,15], *etc*. Nevertheless,

these methods show significant limitations due to the use of organic solvents or poor control over the porous structure (size, shape and interconnectivity). Recently, additive manufacturing (AM) has gained considerable attention because of its capacity to fabricate scaffolds with tailored architecture[16–18]. The process is conducted in a layer-by-layer fashion enabling the formation of a well-defined and highly controlled porous structure[19–21]. On the other hand, chemical etching can create micro pores on the scaffold surface by using inorganic etchants[22]. As some of the material is etched away, pits and protrusions are created on the native smooth surface, resulting in a porous surface topography. However, it is difficult to fabricate the required porous structure by using AM or chemical etching alone, as the smallest pore size by the former method is always tens to hundreds of microns while the porous structure by the latter method only distributes on the scaffolds surface. In view of this deficiency, the efforts in this study were oriented towards investigating the possibility of combining these two techniques to fabricate multi-scale porous scaffolds.

Poly(L-lactic acid) (PLLA) is widely recognized as a promising scaffold material by virtue of its good biocompatibility and process ability[23,24]. It is able to degrade *in vivo* into nontoxic products, which makes it one of the few polymers that obtain the approval of Food and Drug Administration (FDA). However, PLLA is semi-crystalline and highly hydrophobic, resulting in very slow degradation kinetics. It is known that PLLA is susceptible to chemical etching in sodium hydroxide (NaOH) solution[25]. This motivates us to hypothesize that the slow degradation rate of PLLA scaffolds may be adjusted by chemical etching due to the changes of porosity and topography on the scaffolds surface. Moreover, the etching process may also introduce hydrophilic hydroxyl and carboxyl groups to the scaffolds surface, which is beneficial for apatite nucleation. The mechanical strength, on the other hand, inevitably becomes victim to the etching process due to the increased porosity and formation of pits or even cracks on the scaffolds surface. To compensate the mechanical losses and maintain the porous structure, we endeavor to reinforce the porous scaffold by introducing graphene oxide (GO), which has shown great potential as reinforcing agent because of excellent mechanical properties and high surface area[26–28]. To our knowledge, research on the combined process of AM and chemical etching for the fabrication of multi-scale porous scaffold is still a blank area.

In this work, a combined process of AM and chemical etching was developed to fabricate multi-scale porous structure for GO/PLLA scaffold. The porous structure, mechanical properties and degradability of scaffolds were systematically investigated.

2. Materials and methods

2.1 Materials

Medical-grade PLLA powder was purchased from Jinan Daigang Biomaterial Co., Ltd. It had an average molecular weight of 10,000, a glass transition temperature of 60~65 °C, a melting temperature of 175~185 °C and a purity ≥99%. GO powder (diameter of 100~200 nm, thickness of 0.8~1.2 nm, single layer ratio >99% and purity >99%) was produced by Nanjing JCNANO Tech Co., Ltd., China. Analytical-grade NaOH used in this study was obtained from Xilong Chemical Co., Ltd., China. Ultrapure water was used throughout the experimental process.

2.2 AM and chemical etching process

As illustrated in Figure 1, the fabrication process of multi-scale porous scaffolds consisted of three steps, including powder preparation, scaffold fabrication and chemical etching. For the first step, GO/PLLA composite powder was prepared as the raw material for composite scaffolds. More specifically, certain amounts of PLLA and GO powders with a mass ratio of 99:1 were ultrasonically dispersed with continuous stirring in separate containers containing ethanol for 30 min. The resulting suspensions were then mixed together and subject to ultra-sonication and stirring for additional 30 min. Afterwards, the mixed suspension was filtered using Millipore filter, followed by vacuum-drying at 40 °C for 24 h. Finally, the powder was scraped off the filter and crushed in a mortar to obtain GO/PLLA composite powder.

For the second step, the PLLA or GO/PLLA composite powders were used to prepare scaffolds on a self-developed laser AM system[29], with laser power of 5 W, scanning speed of 500 mm•min^{-1} and layer thickness of 0.15 mm. The detailed fabrication process could be described as follows: firstly, a layer of powder was laid on the platform, then a laser was controlled to selectively scan and bond the powder particles according to a predetermined path, after the bottom layer was completed the platform would drop down by a layer's thickness, and a new layer of powder was laid and printed on the former layer, this process would be repeated until the scaffold was obtained. With this process, the pore properties (size, shape, distribution, interconnectivity, *etc*.) of scaffolds could be highly controlled by altering the laser and scanning parameters (laser spot size, scanning space, *etc*.).

For the third step, NaOH solution (concentration of 1 mol•L^{-1}) was prepared by dissolving the aforementioned NaOH in ultrapure water under continuous stirring
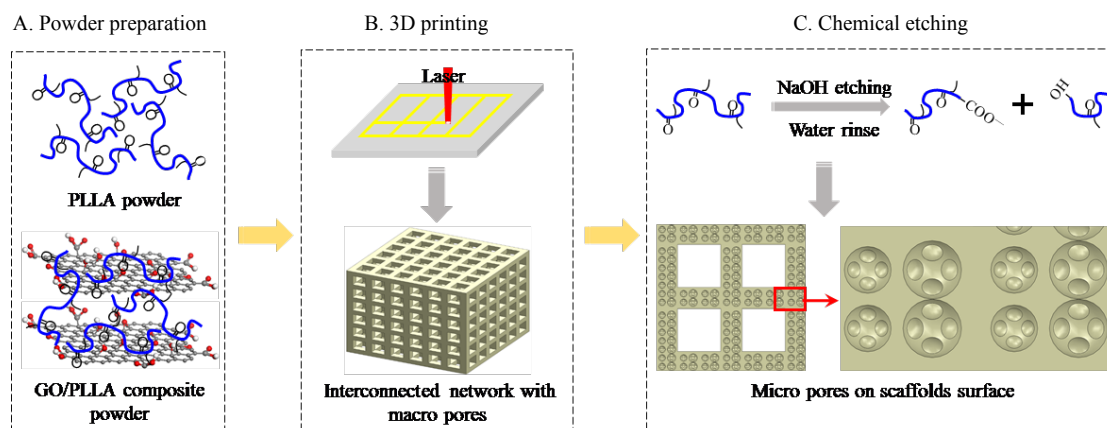
Figure 1. The fabrication process of multi-scale porous scaffolds. (**A**) powder preparation, (**B**) porous scaffolds with macro pores by AM and (**C**) micro pores on scaffolds surface by chemical etching.

for 2 h to ensure complete dissolution and prevent local concentration buildup. Then the scaffolds were subjected to a chemical etching process by immersing them in the NaOH solution under stirring at 37 °C. The weight ratio of NaOH-to-scaffold in the solution was higher than 1000 (1600:1 mole ratio) to ensure a nearly constant pH during the etching process. As depicted in Figure 1C, PLLA could be broken down into two shorter soluble chains with new carboxyl groups and hydroxyl end groups *via* a hydrolysis reaction with NaOH. After chemical etching for different time periods (0.5, 1.0, 1.5 h), the scaffolds were rinsed with ultrapure water to remove residual NaOH and PLLA fragments until the eluant reached a stable pH of 7.0, followed by vacuum-drying at 40 °C for 24 h. For brevity, the scaffolds with or without GO addition were designated as GO/PLLA-x and PLLA-x, respectively, where x corresponded to the etching time in NaOH solution.

2.3 Characterization

The porous scaffolds were sputter coated with a thin platinum layer for imaging by using a field emission scanning electron microscope (FE-SEM, Tescan Mira/LMU, Czech Republic). Phase analysis on the scaffold surfaces was performed using a Rigaku D/MAX 2550V diffractometer with Cu-Kα radiation at a voltage of 40 kV, a current of 250 mA, a scanning speed of 2 °•min⁻¹ and 2θ range of 5°~65°.

The porous scaffolds were subjected to compression tests by using a universal testing machine (WD-D1, Shanghai Zhuoji instruments Co., Ltd., China) equipped with a S-beam load cell at a crosshead speed of 0.5 mm•min⁻¹. The stress-strain curves of the scaffolds were recorded until breakage to determine the compressive strength. Besides, the hardness (HV) of the scaffolds was measured by indentation technique using a digital microhardness tester (HXD-1000TM/LCD, Shanghai

Taiming Optical Instrument Co., Ltd., China). The indentations were made on the scaffolds at a peak load of 2.94 N (300 gf) and a dwell time of 15 s. H_V was then calculated from the indentation data based on Eq. 1:

$$H_V = 0.1891 \frac{P}{d^2} \tag{2.1}$$

where P is the peak load and d is the diagonal length of indentation. For both the compression and indentation tests, five replicates were carried out for each group and the results were averaged.

The degradation behavior of scaffolds was studied by incubation in home-made simulated body fluid (SBF) solution, which consisted of 8.035 g L⁻¹ NaCl, 0.355 g L⁻¹ NaHCO₃, 0.225 g L⁻¹ KCl, 0.231 g L⁻¹ K₂HPO₄•3H₂O, 0.311 g L⁻¹ MgCl₂•6H₂O and 0.292 g L⁻¹ CaCl₂. In brief, all the scaffolds were firstly weighed by using an electronic balance (FA1004, Changzhou Hengzheng Electronic Instrument Co., Ltd., China) and then sterilized with 70% ethanol aqueous solution, which also served as a pre-wetting treatment to enable the subsequent permeation of SBF solution into all of the pores of the scaffolds. Afterwards, the scaffolds were immersed in SBF solution (scaffold/solution ratio of 10 mg/mL) at 37 °C in sealed 12-well plates (LabServ, Thermo Fisher Scientific, USA) under a mild shaking condition. To better mimic the degradation environment *in vivo*, SBF solution was collected and renewed every second day. At week 1, 2, 3, 4, and 5, the scaffolds were collected, gently rinsed with ultrapure water, vacuum-dried at 40 °C for 24 h and then weighed. Weight loss (Δ*Wt*) was calculated according to Eq. 2:

$$\Delta W_t = \frac{W_0 - W_t}{W_0} \times 100\% \tag{2.2}$$

where W_0 is the initial dry weight and W_t is the dry weight at a given time point. Five scaffolds at each

time point were used for the weight. Finally, the surface morphologies and element distributions of the scaffolds at different time points were investigated by FE-SEM and energy dispersive spectroscopy (EDS, X-Max20, Oxford Inc., UK).

2.4 Statistical analysis

All quantitative results were expressed as means ± standard deviations. Statistical analysis was performed between different groups by Student's t-test using SPSS software (SPSS Inc., Chicago, IL, USA). And p values < 0.05 were considered statistically significant.

3. Results

3.1 Multi-scale porous structure

To gain insight into the multi-scale porous structure, FE-SEM analysis was employed to study the porous morphology and size distribution of scaffolds. As presented in Figure 2(a1), the scaffolds exhibited a well-defined porous network in three dimensions comprising interconnected pores, with an average pore size of 948±74 μm. Clearly, the chemical etching process did not alter the original interconnected porous structure of the scaffolds (Figures 2(a2), 2(a3) and 2(a4)). Moreover, further observations revealed that the scaffold without chemical etching had a smooth surface while those chemically treated scaffolds exhibited a progressively

roughened surface feature with the extension of etching time. This was attributed to the non-homogeneous hydrolysis of PLLA caused by the non-uniform local crystallinity and cross-linking on the scaffolds surface. Subtle morphological variations were revealed at higher-magnification images. It was found that the chemical etching process introduced micro pores (pits and protrusions) throughout the struts of the scaffolds due to the cleavage of ester bonds. A short etching time of 0.5 h produced some surface pores with characteristic sizes of 1~2 μm. As the etching time increased to 1.0 h, more PLLA was hydrolyzed, leaving well-ordered pore arrangement on the scaffold surface with pore size ranging from 1 μm to 3 μm. Moreover, these pores were penetrated by smaller pores with pore size less than 1 μm. In comparison, extending etching time to 1.5 h led to numerous pores with a range of sizes ranging from 1 μm to 10 μm on the struts. Such an increase of surface roughness demonstrated a time-dependent etching degree and higher hydrophilicity compared to PLLA-0 scaffold, facilitating the adhesion and ingrowth of cells[30]. However, many cracks appeared on the scaffold surface after 1.5 h of etching, which implied that excessive etching might damage the original surface porous network or even the structure of bulk scaffold. These results confirmed that the multi-scale porous structure could be fabricated and regulated by altering the parameters of AM and chemical etching.
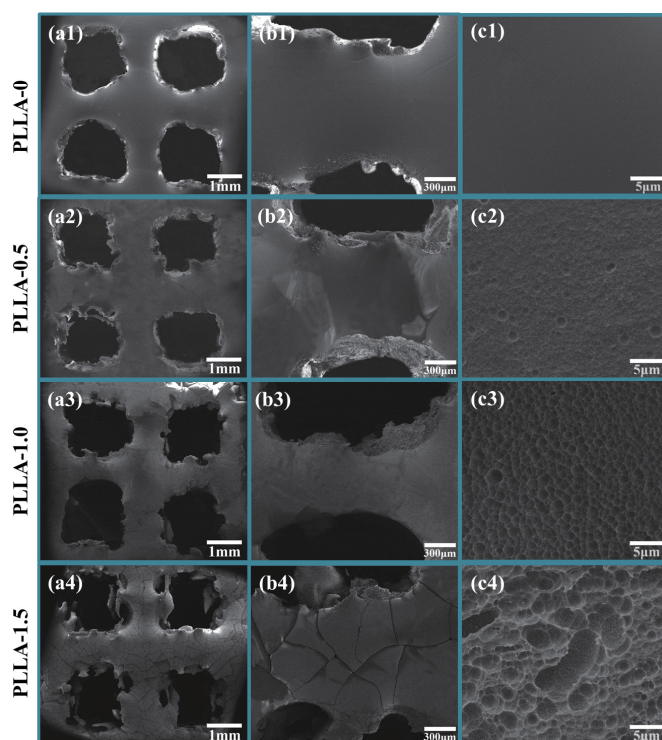

Figure 2. FE-SEM characterization of the multi-scale porous scaffolds: (a) interconnected porous network by AM, (b) Low- and (c) high-magnification images of porous surface structure by chemical etching for different etching time.

3.2 Phase composition

The phase composition of scaffolds was analyzed using X-ray diffraction (XRD) within a wide 2θ range of 5°~65° (Figure 3). Results presented typical broadened patterns dominated by two diffraction peaks located at 16.6° and 19.1°, which could been ascribed to the semi-crystalline nature of PLLA. After NaOH etching process, no new diffraction peaks were detected, demonstrating the NaOH etching process did not lead to phase change.

3.3 Mechanical properties

Compression tests were performed to quantify the effect of chemical etching on the mechanical properties of the multi-scale porous scaffolds. Figure 4(a) showed the representative stress-strain curves of the scaffolds under compression tests. It could be seen that the stress of PLLA-0 scaffold had a sudden drop at a maximum of 20.1 MPa, indicating the brittleness nature of PLLA. In comparison, the maximum stress of scaffolds after chemical etching gradually decreased. It was not surprising that the chemical etching process had a negative effect on the compressive properties of scaffold due to the increased porosity on scaffold surface. The relationship between the compressive strength on etching time was presented in Figure 4(b). As the etching time increased from 0 h to 1.5 h, the compressive strength of the scaffolds was considerably decreased by 30.1% from 22.2 ± 1.7 MPa to 15.5 ± 1.5 MPa. It was well known that scaffolds should have adequate mechanical properties to provide structural support for the new tissues after implantation[8]. Therefore, to compensate

the mechanical loss caused by chemical etching, 1 wt% GO was incorporated into the PLLA scaffolds. The typical microstructure of GO/PLLA scaffold before chemical etching was presented in Figure 4(c). It could be seen that after the addition of GO, the GO/PLLA scaffold also exhibited a smooth and dense surface, showing no obvious differences compared with PLLA scaffold shown in Figure 2(c1). The surface porous structure of GO/PLLA-1.0 scaffold was presented in Figure 4(d). Similarly, little differences in the micropore structure were observed between the etched GO/PLLA-1.0 scaffold and PLLA-1.0 scaffold. The compressive stress for GO/PLLA-0, GO/PLLA-0.5, GO/PLLA-1.0, and GO/PLLA-1.5 were 32.2 ± 1.3 MPa, 28.3 ± 1.2 MPa, 24.5 ± 2.1 MPa, 19.7 ± 2.3 MPa, respectively. Clearly, the incorporation of GO considerably improved the mechanical properties of the etched scaffolds. Specifically, the compressive strength of GO/PLLA-1.0 scaffold was approximately 41.6% and 10.3% higher than that of PLLA-1.0 scaffold and PLLA-0 scaffold, respectively. Moreover, the strength of fabricated scaffolds was comparable to or even higher than that of cancellous bone (4-20 MPa)[31].

Subsequent indentation tests revealed a similar trend of the hardness with that of compressive strength, as showed in Figure 5. The hardness of PLLA-0 scaffold could reach 22.21 ± 0.84 Hv, whereas the porous surface structure by chemical etching impaired the hardness of scaffolds, *e.g.* after etching for 1.5 h the hardness decreased by 18.7% to 18.05 ± 1.41 Hv in comparison to PLLA-0 scaffold. However, the hardness of scaffolds
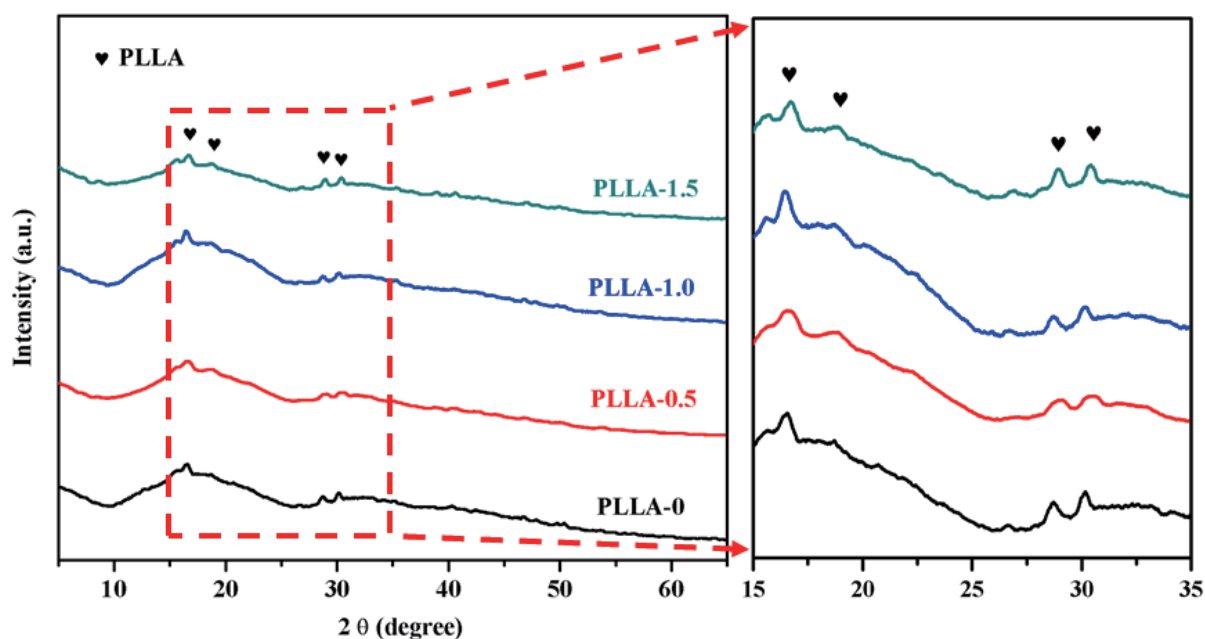

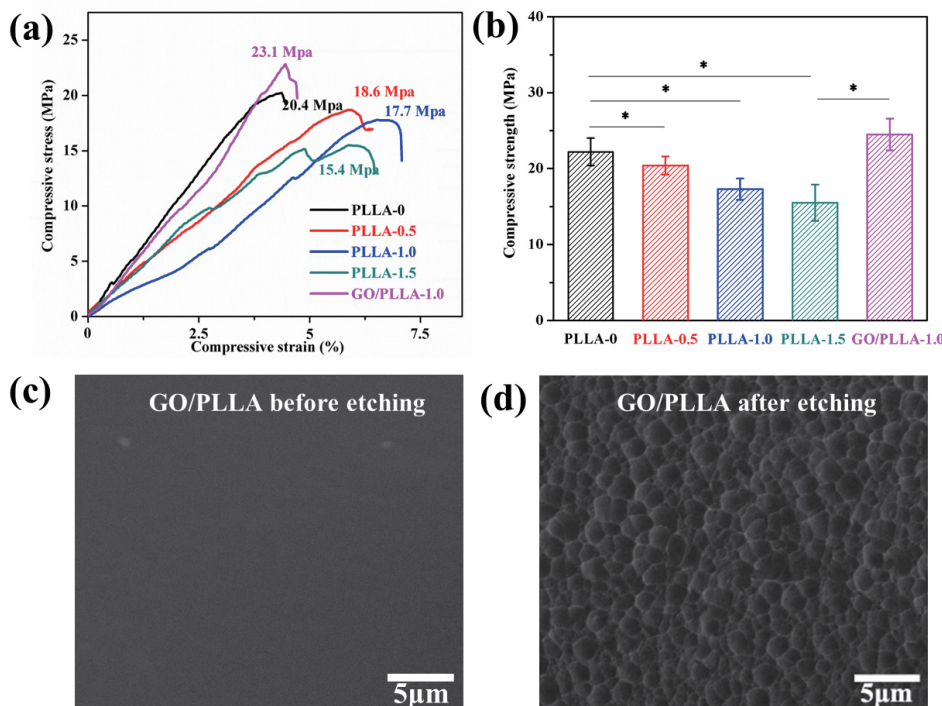**Figure 3.** XRD analysis of the phase composition of the scaffolds with and without chemical etching.

Figure 4. (a) Representative stress-strain curves and (b) compressive strength of the scaffolds under compression tests. Asterisks denote significant difference with $p < 0.05$, as compared with PLLA-0 scaffold. $n = 5$. The typical surface microstructure of (c) GO/PLLA scaffold and (d) GO/PLLA-1.0 scaffold.
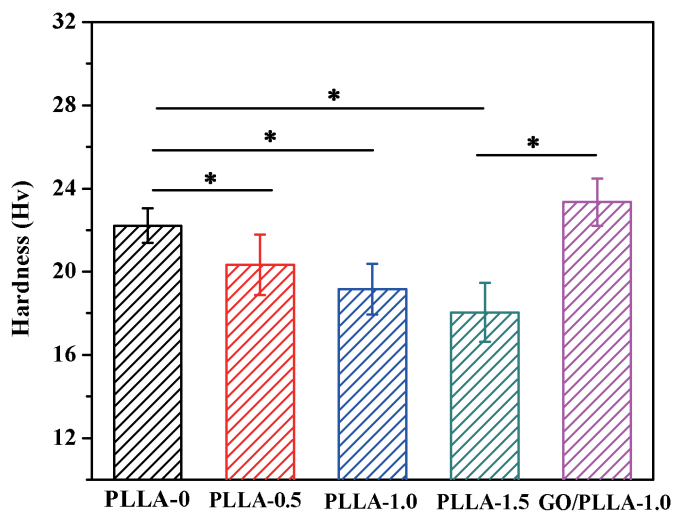

Figure 5. Relationship between the hardness of scaffolds and etching time. Asterisks denote significant difference with $p < 0.05$, as compared with PLLA-0 scaffold. $n = 5$.

was distinctly improved after the incorporation of GO. Particularly, GO/PLLA-1.0 scaffold exhibited a 21.8% increase of hardness to 23.34 ± 1.14 Hv compared with PLLA-1.0 scaffold (19.16 ± 1.21 Hv). Such a significant reinforcement of PLLA-x scaffolds is believed to result from the strong polymer-GO interface and reinforcing mechanisms by GO[32], which could slow down the crack propagation in the scaffolds under load. And the hardness of fabricated scaffolds was comparable to that

of cancellous bone (20-30 Hv)[31].

3.4 Biodegradation and mineralization

The multi-scale porous scaffolds were immersed in SBF solution to investigate the degradability and bioactivity. As shown in Figure 6, PLLA-0 scaffold had a stable degradation curve over 5 weeks of immersion. It underwent little weight loss during the first week and degraded slightly about $6.6\% \pm 1.3\%$ until 5 weeks. In
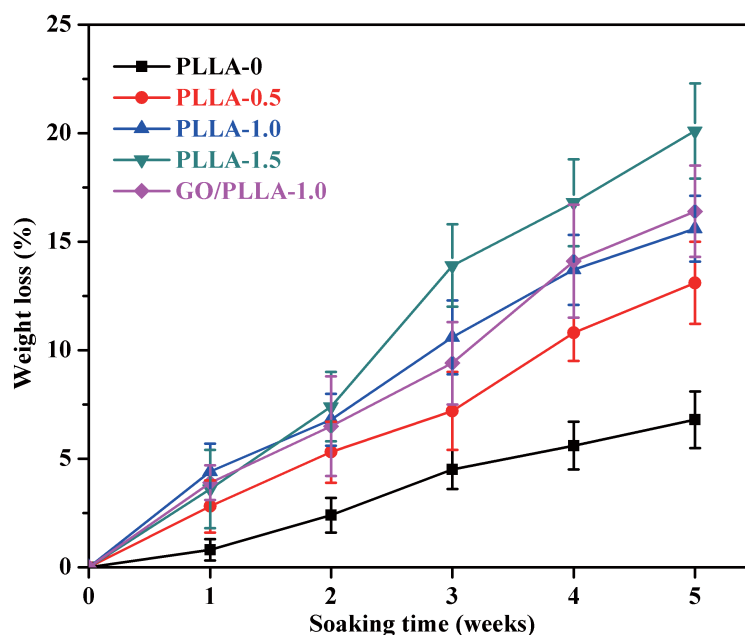
Figure 6. Weight loss of the multi-scale porous scaffolds in SBF solution. Error bars represent the standard deviation. *n* = 3.

contrast, the chemically etched scaffolds demonstrated accelerated degradation rates with increasing chemical etching time. Specifically, PLLA-0.5 and PLLA-1.5 scaffolds lost 2.8% and 4.4% of their initial weights after the first 1 week of immersion. Then the weight loss showed a continuous increase in the subsequent weeks. After 5 weeks, the weight loss of PLLA-0.5 scaffold was about 13.1 ± 1.9%, whereas the weight losses for PLLA-1.0 and PLLA-1.5 scaffolds rapidly increase to 15.6 ± 1.5% and 20.1 ± 2.2%, respectively. These kinetic trends indicated that the complete degradation of PLLA scaffolds could be regulated from a few months to a year by altering the porous structure according to specific needs. In addition, the addition of GO showed no obvious effect on the degradation rate of PLLA scaffolds.

In view of the hydrophilic hydroxyl and carboxyl groups on PLLA-*x* scaffolds, it was necessary to evaluate their bioactivity in terms of apatite-forming ability by SBF tests. Thus, the degradation morphology and element distribution of scaffolds after immersion for 5 weeks were studied by FE-SEM/EDS (Figure 7). Figures 7(a1) and 7(b1) showed no apparent deposits on PLLA-0 scaffold after immersion due to its hydrophobicity. Interestingly, Figure 7(a2) showed that some spheres formed on the surface of PLLA-0.5 scaffold. The chemical analysis of these spheres by EDS (Figure 7(c2)) revealed typical peaks of calcium and phosphate with a Ca/P atomic ratio of 1.5, indicating the formation of apatite crystals[33]. With increasing chemical etching time, the amount of apatite crystals on scaffolds surface increased, which could be attributed to the

increased hydrophilic groups and contact area between the scaffolds and solution. In the case of GO/PLLA-1.0 scaffold, almost a layer of apatite could be observed on the scaffold surface owing to more nucleation sites provided by GO. This was also confirmed by the stronger peaks of calcium and phosphate displayed in Figure 7(c5) as compared with PLLA-*x* scaffolds. These results indicated that both the degradability and bioactivity of PLLA scaffolds could be moderated by altering the porous structure *via* AM and chemical etching.

4. Discussion

In this study, interconnected porous PLLA scaffolds were fabricated by AM, and then chemical etching was used to obtain porous structure on the scaffolds surface *via* selective hydrolysis in NaOH solution. It was well accepted that the crystalline regions in PLLA were more difficult to cleave by alkaline treatment than the amorphous regions. Thus, the hydroxyl anions in NaOH solution would primarily attack the carbonyl groups in the amorphous regions of PLLA, leading to the cleavage of ester bonds into water-soluble oligomers or shorter polymer chains with polar groups. Along with the dissolution of these oligomers and short chains, micro pores formed on the scaffolds surface. There were many kinds of pore structure, including surface pores, inside pores, *etc*. In our study, the chemical etching process introduced micro surface pores throughout the struts of the scaffolds. And smaller pores with pore size less than 1 μm penetrated these surface micro pores. Although they were not fully interconnected, similar structure have also been prepared and named as surface pore structure
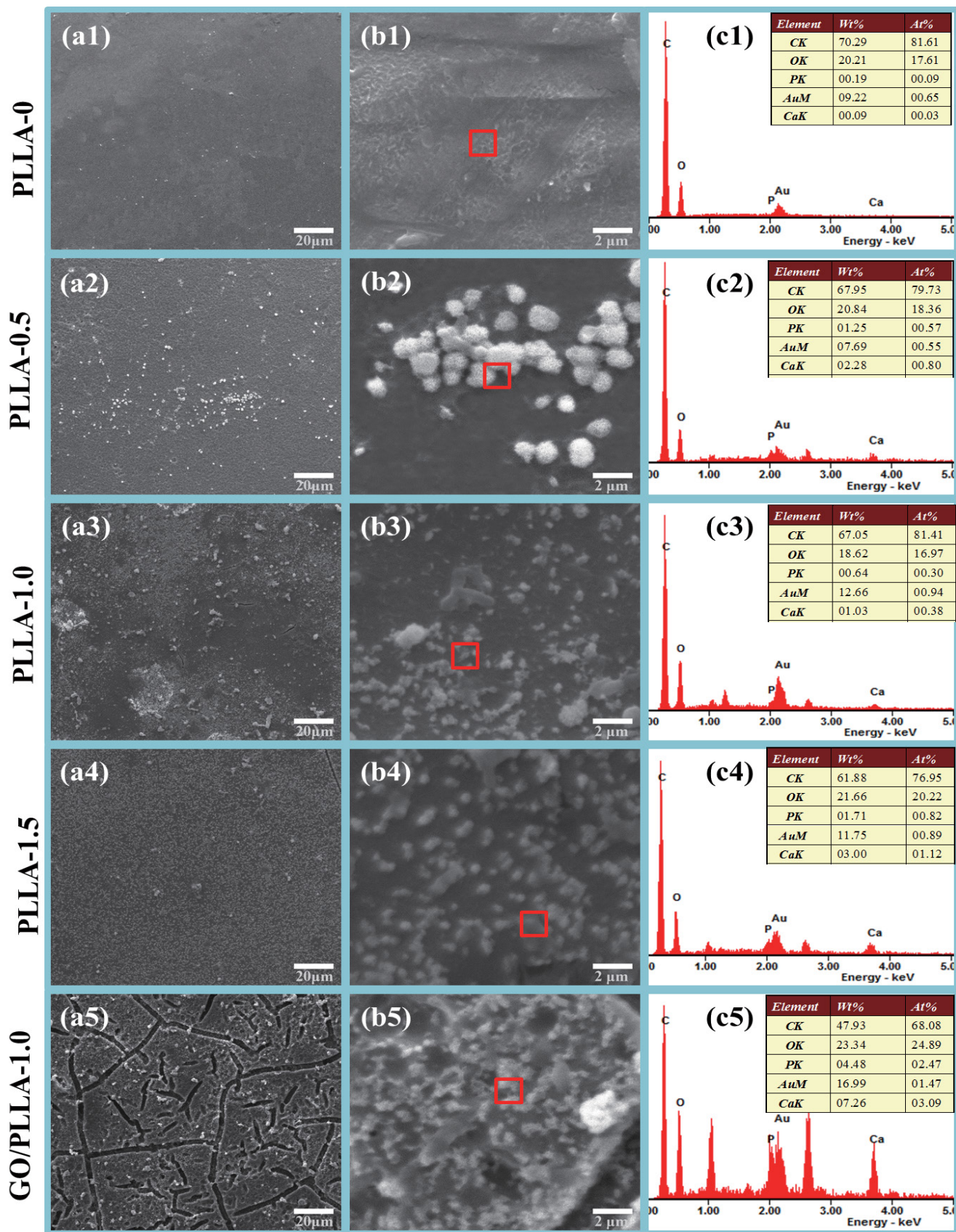
Figure 7. Surface morphology and corresponding EDS results of multi-scale porous scaffolds after immersion in SBF for 5 weeks.

by many other studies. For example, Park *et al.* used chemical etching to create surface pores on the PLGA scaffolds[34]. Gautier *et al.* constructed surface pores on silicon layers by chemical treatment[35]. Yerokhov *et al.* developed macroporous crater-like surface on silicon by chemical and electrochemical etching[36]. As revealed by the FE-SEM analysis in our study, the hydrolysis reactions could be promoted with prolonged etching time, leading to increased pore number and pore size in both depth and width. But on the other hand, excessive etching resulted in the damage of original porous network or even shrinkage-induced cracks, thereby deteriorating the properties of the polymer scaffolds.

Once the scaffolds were immersed in SBF solution, the micro pores on scaffolds surface allowed more contact of the scaffolds with the molecules in SBF, resulting in accelerated degradation rate. Moreover, the slopes of the degradation curves changed over time, indicating a variation in the degradation mechanism from an initial low ion diffusion at early stage to a faster network degradation at prolonged immersing times. In addition, the formed polar hydroxyl and carboxyl groups on scaffolds surface could attract the calcium cations in SBF solution and acted as nucleation sites for initial apatite formation. Thus it was easy to understand that both the degradation rate and bioactivity of the scaffolds were controllable by varying the chemical etching time. It should be noted that the micropores obtained by chemical etching improved the surface activity *via* accelerated apatite deposition, which contributed to forming good bone/scaffold interface bonding[37–39]. Meanwhile, the micropores increased the surface roughness and thus could significantly facilitate cell adhesion and resultantly bone tissue growth[40–42]. Moreover, the formed micropores accelerated the degradation rate of the scaffold. There was no doubt that timely degradation is important to the healing of bone defects. Therefore, these surface micropores were certainly beneficial for bone tissue regeneration.

However, the mechanical properties of PLLA scaffolds were significantly decreased after the alkaline treatment due to the increased porosity. Thus, GO was incorporated to enhance the mechanical properties of PLLA scaffolds. It was well accepted that the microstructure and porosity had a significant effect on the mechanical properties of scaffolds. Nevertheless, little differences in the microstructure and porosity were observed between the etched scaffolds with and without GO, as presented in Figures 2 and 4. In fact, the size of surface micropores obtained by chemical etching was about 1-2 microns, which was 2-3 orders of magnitude different from the macropores (hundreds of microns) constructed by AM. Therefore, the porosity of the scaffold mainly depended on the macropores constructed by AM, instead of the

micropores obtained by chemical etching. Moreover, the macropore structure of the scaffolds was determined by the AM parameters, including laser spot size, hatch spacing, *etc*. Therefore, at the same AM parameters, there was no obvious differences in porosity between the scaffolds with and without GO. In this study, GO/PLLA scaffolds exhibited a much higher compressive strength, which might be ascribed to the reinforcing mechanisms by GO, such as crack bridging[43] and pull-out[44], enabling the efficient absorption and dissipation of stress in the scaffolds. More importantly, the addition of GO provided more active sites for apatite nucleation, thereby further improving the bioactivity of PLLA scaffolds. The biocompatibility of PLLA and GO/PLLA scaffolds has been studied using CCK 8 assays in our previous study. And the results reveled that PLLA/GO scaffold had better biocompatibility than PLLA scaffold. The stimulatory effect of GO on cell behavior was attributed to the oxygen-containing functional groups on GO surface that could promote cell proliferation[45–47].

5. Conclusions

A combined process of AM and chemical etching was developed to fabricate multi-scale porous scaffolds. By modulating the parameters of AM and chemical etching, the GO/PLLA scaffolds possessed: (i) controllable multi-scale porous structure, that was interconnected macro pores and surface micro pores; (ii) tunable degradation rate ranging from a few months to a year; (iii) favorable bioactivity resulting from the formed polar groups and GO; (iv) adjustable mechanical strength in a range of 15.5~24.5 MPa. The combined process in this study could be extended to other polymer-based scaffolds and was expected to provide a new strategy for developing porous scaffolds.

Conflict of Interest and Funding

References

1. Tavolaro P, Catalano S, Martino G, *et al*., 2016, Zeolite inorganic scaffolds for novel biomedical application: Effect of physicochemical characteristic of zeolite membranes on cell adhesion and viability. *Appl Surf Sci*, 380: 135–140. http://doi.org/10.1016/j.apsusc.2016.01.279

2. Puppi D, Piras A M, Pirosa A, *et al*., 2016, Levofloxacin-loaded star poly(ε-caprolactone) scaffolds by additive manufacturing. *J Mater Sci Mater Med*, 27(3): 44. http://doi.org/10.1007/s10856-015-5658-1

3. Fradique R, Correia T R, Miguel S P, *et al*., 2016, Production of new 3D scaffolds for bone tissue regeneration by rapid prototyping. *J Mater Sci Mater Med*, 27(4): 1–14. http://doi.org/10.1007/s10856-016-5681-x

4. Gao C, Deng Y, Feng P, *et al*., 2014, Current progress in bioactive ceramic scaffolds for bone repair and regeneration. *Int J Mol Sci*, v15(3): 4714–4732. http://doi.org/10.3390/ijms15034714

5. Yuan H, Zhou Q, Li B, *et al*., 2015, Direct printing of patterned three-dimensional ultrafine fibrous scaffolds by stable jet electrospinning for cellular ingrowth. *Biofabrication*, 7(4): 045004. http://doi.org/10.1088/1758-5090/7/4/045004

6. Gao C, Peng S, Feng P, *et al*., 2017, Bone biomaterials and interactions with stem cells. *Bone Res*, 21; 5: 17059. http://doi.org/10.1038/boneres.2017.59

7. Ng R, Zhang X, Liu N, *et al*., 2009, Modifications of nonwoven polyethylene terephthalate fibrous matrices *via* NaOH hydrolysis: Effects on pore size, fiber diameter, cell seeding and proliferation. *Process Biochem*, 44(9): 992–998. http://doi.org/10.1016/j.procbio.2009.04.024

8. Bose S, Roy M, Bandyopadhyay A, 2012, Recent advances in bone tissue engineering scaffolds. *Trends Biotechnol*, 30(10): 546. http://doi.org/10.1016/j.tibtech.2012.07.005

9. Inzana J A, Olvera D, Fuller S M, *et al*., 2014, 3D printing of composite calcium phosphate and collagen scaffolds for bone regeneration. *Biomaterials*, 35(13): 4026–4034. http://doi.org/10.1016/j.biomaterials.2014.01.064

10. Sun H, Zhu F, Hu Q, *et al*., 2014, Controlling stem cell-mediated bone regeneration through tailored mechanical properties of collagen scaffolds. *Biomaterials*, 35(4): 1176–1184. http://doi.org/10.1016/j.biomaterials.2013.10.054

11. Zhang X, Zhang Y, Ma G, *et al*., 2015, The effect of prefrozen process on properties of chitosan/ hydroxyapatite/ poly(methyl methacrylate) composite prepared by freeze drying method used for bone tissue engineering. *RSC Adv*, 5(97): 79679–79686. http://doi.org/10.1039/C5RA14549J

12. Sultana N, Wang M, 2012, PHBV/PLLA-based composite scaffolds fabricated using an emulsion freezing/freeze-drying technique for bone tissue engineering: surface modification and *in vitro* biological evaluation. *Biofabrication*, 4(1): 015003. http://doi.org/10.1088/1758-5082/4/1/015003

13. Soh E, Kolos E, Ruys A J, 2015, Foamed high porosity alumina for use as a bone tissue scaffold. *Ceram Int*, 41(1): 1031–1047. https://doi.org/10.1016/j.ceramint.2014.09.026

14. Wang C, Chen H, Zhu X, *et al*., 2017, An improved polymeric sponge replication method for biomedical porous titanium scaffolds. *Mater Sci Eng C Mater Biol Appl*, 70(Pt 2): 1192. http://doi.org/10.1016/j.msec.2016.03.037

15. Baino F, Vitale-Brovarone C, 2014, Mechanical properties and reliability of glass–ceramic foam scaffolds for bone repair. *Mater Lett*, 118(3): 27–30. https://doi.org/10.1016/j.matlet.2013.12.037

16. Kumar A, Mandal S, Barui S, *et al*., 2016, Low temperature additive manufacturing of three dimensional scaffolds for bone-tissue engineering applications: Processing related challenges and property assessment. *Mater Sci Eng R Rep*, 103: 1–39. https://doi.org/10.1016/j.mser.2016.01.001

17. Yang Y, Wu P, Lin X, *et al*., 2016, System development, formability quality and microstructure evolution of selective laser-melted magnesium. *Virtual Phys Prototyp*, 11(3): 173–181. http://doi.org/10.1080/17452759.2016.1210522

18. Ng W L, Goh M H, Yeong W Y, *et al*., 2018, Applying macromolecular crowding to 3D bioprinting: Fabrication of 3D hierarchical porous collagen-based hydrogel constructs. *Biomater Sci*, 6(3): 562–574. http://doi.org/10.1039/c7bm01015j

19. Pei F, Peng S, Ping W, *et al*., 2016, A nano-sandwich construct built with graphene nanosheets and carbon nanotubes enhances mechanical properties of hydroxyapatite–polyetheretherketone scaffolds. *Int J Nanomed*, 11: 3487–3500. http://doi.org/10.2147/IJN.S110920

20. Shuai C, Guo W, Gao C, *et al*., 2017, An nMgO containing scaffold: Antibacterial activity, degradation properties and cell responses. *Int J Bioprint*, 4(1): 120. http://dx.doi.org/10.18063/IJB.v4i1.120

21. Deng Y, Yang Y, Gao C, *et al*., 2018, Mechanism for corrosion protection of β-TCP reinforced ZK60 *via* laser rapid solidification. *Int J Bioprint*, 4(1): 124. http://dx.doi.

org/10.18063/IJB.v4i1.124

22. Wang Z, Macosko C W, Bates F S, 2014, Tuning surface properties of poly(butylene terephthalate) melt blown fibers by alkaline hydrolysis and fluorination. *ACS Appl Mater Interfaces*, 6(14): 11640. http://doi.org/10.1021/am502398u

23. Pei F, Peng S, Ping W, *et al.*, 2016, A space network structure constructed by tetraneedlelike ZnO whiskers supporting boron nitride nanosheets to enhance comprehensive properties of poly(L-lacti acid) scaffolds. *Sci Rep*, 6: 33385. http://doi.org/10.1038/srep33385

24. Cardea S, Baldino L, Pisanti P, *et al.*, 2014, 3-D PLLA scaffolds formation by a supercritical freeze extraction assisted process. *J Mater Sci Mater Med*, 25(2): 355–362. http://doi.org/10.1007/s10856-013-5069-0

25. Peng F, Olson J R, Shaw M T, *et al.*, 2009, Influence of pretreatment on the surface characteristics of PLLA fibers and subsequent hydroxyapatite coating. *J Biomed Mater Res B Appl Biomater*, 88(1): 220. http://doi.org/10.1002/jbm.b.31172

26. Wang H, Qiu Z, 2012, Crystallization kinetics and morphology of biodegradable poly(l-lactic acid)/graphene oxide nanocomposites: Influences of graphene oxide loading and crystallization temperature. *Thermochim Acta*, 527(1): 40–46.

27. Shuai C, Feng P, Wu P, *et al.*, 2016, A combined nanostructure constructed by graphene and boron nitride nanotubes reinforces ceramic scaffolds. *Chem Eng J,* 313: 487–497. https://doi.org/10.1016/j.cej.2016.11.095

28. Gao C, Pei F, Peng S, *et al.*, 2017, Carbon nanotubes, graphene and boron nitride nanotubes reinforced bioactive ceramics for bone repair. *Acta Biomater*, 61: 1–20. https://doi.org/10.1016/j.actbio.2017.05.020

29. Shuai C, Gao C, Nie Y, *et al.*, 2011, Structure and properties of nano-hydroxypatite scaffolds for bone tissue engineering with a selective laser sintering system. *Nanotechnology*, 22(28): 285703. http://doi.org/10.1088/0957-4484/22/28/285703

30. Wu D, Xu F, Sun B, *et al.*, 2012, Design and preparation of porous polymers. *Chem Rev*, 112(7): 3959.

31. Johnson A J W, Herschler B A, 2011, A review of the mechanical behavior of CaP and CaP/polymer composites for applications in bone replacement and repair. *Acta Biomater*, 7(1): 16–30. http://doi.org/10.1016/j.actbio.2010.07.012

32. Shuai C, Feng P, Gao C, *et al.*, 2015, Graphene oxide reinforced poly(vinyl alcohol): Nanocomposite scaffolds for tissue engineering applications. *RSC Adv*, 5(32): 25416–25423. http://doi.org/10.1039/C4RA16702C

33. Li Y, Wang F, Yang J, *et al.*, 2007, *In vitro* synthesis and characterization of amorphous calcium phosphates with various Ca/P atomic ratios. *J Mater Sci Mater Med*, 18(12): 2303–2308. http://doi.org/10.1007/s10856-007-3132-4

34. Park G E, Pattison M A, Park K, *et al.*, 2005, Accelerated chondrocyte functions on NaOH-treated PLGA scaffolds. *Biomaterials*, 26(16):3075–3082. http://doi.org/10.1016/j.biomaterials.2004.08.005

35. Gautier G, Kouassi S, Desplobain S, *et al.*, 2012, Macroporous silicon hydrogen diffusion layers for micro-fuel cells: From planar to 3D structures. *Microelectron Eng*, 90(2):79–82. https://doi.org/10.1016/j.mee.2011.04.003

36. Yerokhov V Y, Hezel R, Lipinski M, *et al.*, 2002, Cost-effective methods of texturing for silicon solar cells. *Sol Energy Mater Sol Cells*, 72(1–4):291–298. https://doi.org/10.1016/S0927-0248(01)00177-5

37. Dinarvand P, Seyedjafari E, Shafiee A, *et al.*, 2011, New approach to bone tissue engineering: Simultaneous application of hydroxyapatite and bioactive glass coated on a poly(L-lactic acid) scaffold. *ACS Appl Mater Interfaces*, 3(11): 4518–4524. http://doi.org/10.1021/am201212u

38. Wang Z, Xu Y, Wang Y, *et al.*, 2016, Enhanced *in vitro* mineralization and *in vivo* osteogenesis of composite scaffolds through controlled surface grafting of L-lactic acid oligomer on nanohydroxyapatite. *Biomacromolecules*, 17(3): 818–829. http://doi.org/10.1021/acs.biomac.5b01543

39. Liu F, Qiu W, Wang H, *et al.*, 2013, Biomimetic deposition of apatite coatings on biomedical NiTi alloy coated with amorphous titanium oxide by microarc oxidation. *Mater Sci Technol*, 29(6): 749–753. https://doi.org/10.1179/1743284712Y.0000000196

40. Jiao Y-P, Cui F-Z, 2007, Surface modification of polyester biomaterials for tissue engineering. *Biomed Mater*, 2(4): R24. http://doi.org/10.1088/1748-6041/2/4/R02

41. Wu S, Liu X, Yeung K W, *et al.*, 2014, Biomimetic porous scaffolds for bone tissue engineering. *Mater Sci Eng R Rep*, 80: 1–36. https://doi.org/10.1016/j.mser.2014.04.001

42. Xia L, Feng B, Wang P, *et al.*, 2012, *In vitro* and *in vivo* studies of surface-structured implants for bone formation. *Int J Nanomed*, 7: 4873. http://dx.doi.org/10.2147/IJN.S29496

43. An Y, Xu X, Gui K, 2016, Effect of SiC whiskers and graphene nanosheets on the mechanical properties of ZrB_2-SiCw-Graphene ceramic composites. *Ceram Int*, 42(12): 14066–14070. https://doi.org/10.1016/j.ceramint.2016.06.014

44. Gao C, Liu T, Shuai C, *et al.*, 2014, Enhancement mechanisms of graphene in nano-58S bioactive glass scaffold: Mechanical and biological performance. *Sci Rep*, 4(4): 4712. https://doi.org/10.1038/srep04712

45. Depan D, Girase B, Shah J, *et al.*, 2011, Structure–process–property relationship of the polar graphene oxide-mediated cellular response and stimulated growth of osteoblasts on hybrid chitosan network structure nanocomposite scaffolds. *Acta Biomater*, 7(9): 3432–3445. https://doi.org/10.1016/j.actbio.2011.05.019

46. Guo C X, Zheng X T, Lu Z S, *et al.*, 2010, Biointerface by cell growth on layered graphene–artificial peroxidase–protein nanostructure for *in situ* quantitative molecular detection. *Adv Mater*, 22(45): 5164–5167. https://doi.org/10.1002/adma.201001699

47. Liu Y, Yu D, Zeng C, *et al.*, 2010, Biocompatible graphene oxide-based glucose biosensors. *Langmuir*, 26(9): 6158–6160. https://doi.org/10.1021/la100886x